Simulation of turbulent exchange processes in summertime leads

Eric D. Skyllingstad and Clayton A. Paulson
College of Oceanic and Atmospheric Sciences, Oregon State University, Corvallis, Oregon, USA

W. Scott Pegau
Kachemak Bay Research Reserve, Homer, Alaska, USA

Received 24 May 2004; revised 8 October 2004; accepted 21 February 2005; published 28 May 2005.

[1] Ice-ocean heat exchange in polar leads was examined using a large-eddy simulation model coupled to a slab ice model. Simulations were performed using an idealized square domain for a range of lead sizes, surface wind stress (0.05–0.1 N m^{-2}), and lead temperature/salinity profiles. Particular emphasis was placed on understanding the role of fresh water in leads and how stratification controls the heat budget and ice edge melting rate. With uniform initial conditions we found that solar heating was not strong enough to develop lead freshening via ice edge melting; even weak winds (0.02 N m^{-2}) generated circulations that maintained a well-mixed lead. In the weak wind case, adding a fresh water flux representative of surface melt runoff provided enough additional stratification so that the lead water became isolated from the rest of the simulated ocean boundary layer. However, stronger winds (0.1 N m^{-2}) prevented the fresh water layer from forming. Experiments initialized with temperature/salinity profiles similar to observed cases (fresh water layer capping the lead) demonstrated that lateral melting rates increase with expanding lead size, agreeing with simple heat balance calculations for a square lead without vertical mixing. However, with stronger winds, lateral melting rates decreased because of greater turbulent mixing of cold water from beneath the fresh layer. Inspection of the lead circulation indicated that the strongest melting occurred where the ice edge currents were the largest. Overall, melting fluxes for a 24 m^2 lead ranged from 200 to 400 W m^{-2}, depending on the wind speed. Without the fresh layer, fluxes ranged from 50 to 60 W m^{-2}, suggesting that fresh water stratification can have a dominate role in controlling ice edge melting.

Citation: Skyllingstad, E. D., C. A. Paulson, and W. S. Pegau (2005), Simulation of turbulent exchange processes in summertime leads, *J. Geophys. Res.*, *110*, C05021, doi:10.1029/2004JC002502.

1. Introduction

[2] Accurate prediction of sea ice coverage is crucial for realistic climate simulation. Sea ice provides an insulative cap on the polar ocean, reducing outgoing heat flux in the winter and incoming solar radiation during the summer. If sea ice coverage declines during the summer months in response to climate change, then solar radiation normally reflected back to space by the ice surface could instead be absorbed by the upper ocean, leading to further melting. Because of this possible feedback, understanding how open water or leads are created in pack ice is critically important in assessing the polar ocean heat budget and changes in the Earth's climate system.

[3] Establishing the typical behavior of leads was an important goal of the Surface Heat Budget of the Arctic experiment (SHEBA). Measurements of ocean properties and lead characteristics were obtained throughout the year-long SHEBA field experiment, with particular focus on the summer melting period. Most leads are formed by dynamic motion of the pack ice produced by winter storms. These leads refreeze, but have an ice draft less than the surrounding ice and typically are the first to open during the summer melt period. At the beginning of summer, leads have seawater properties similar to the underlying ocean boundary layer. As snow melt intensifies in early summer, fresh water pours off of the pack ice into the leads forming a two layer lead water structure characterized by a very fresh surface layer that is initially trapped in the leads.

[4] During the SHEBA summer period, freshening of leads began in June and continued through the month of July until a stormy period late in the month reestablished a well-mixed ocean boundary layer. Solar radiation entering leads during this period of time produced strong heating of the water trapped in the lead and increased lateral melting at the lead edge. For one typical lead referred to as Sarah's Lake, W. S. Pegau and C. A. Paulson (Summertime thermohaline evolution of an Arctic lead, submitted to *Journal of Geophysical Research*, 2005, hereinafter referred to as Pegau and Paulson, submitted manuscript, 2005) estimated a net average heat flux into edge melting of ~820 W m^{-2},

0148-0227/05/2004JC002502$09.00

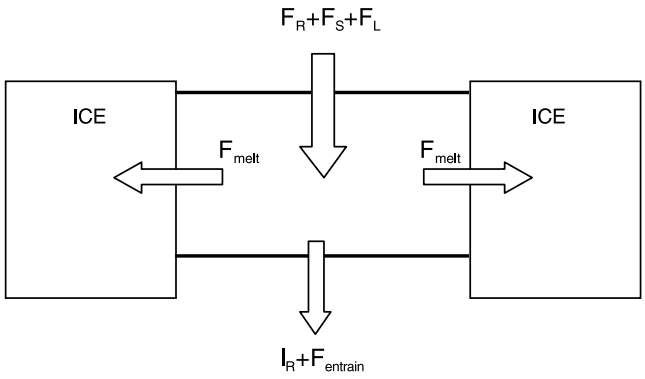

Figure 1. Schematic showing heat fluxes affecting lead heat content and lateral melting.

yielding a melting rate of 0.14–0.23 m d^{-1}, depending on the assumed contact length of the warm fresh layer. These estimates are very large when compared with bottom melt rates of ~0.5–1.0 cm d^{-1} [*Perovich et al.*, 2003], however the area of bottom melting is many times larger than the lead edge area so that the total lateral melting is almost negligible for the total ice mass in comparison with the bottom and surface melt (this can be shown by comparing the ratio of the lead edge area to the total bottom area for a 0.05 lead fraction). Nevertheless, because lateral melting affects the albedo by increasing the size of leads, it is important to understand the turbulent processes that transport solar heat absorbed in the middle of the lead to the edges where melting occurs.

[5] The numerical experiments described here are a first step in developing a more representative parameterization of lead processes for use in coupled climate models. Simple experiments, such as examining the effect of wind speed on lateral melting rates, are needed to develop enough understanding so that physically based parameterizations can be constructed. Contemporary sea ice models typically treat leads as extensions of the underlying ocean mixed layer and set lead temperature and salinity to the mixed layer values [*Holland et al.*, 1997; *Bitz et al.*, 2001]. Accordingly, lateral melt rates are set by the mixed layer properties and do not account for trapped fresh water as observed during SHEBA.

[6] Observations from SHEBA suggest that improved parameterization of lateral melt rates require better estimates of the combined fluxes affecting the lead heat content as shown schematically in Figure 1. The main fluxes are incoming solar radiation (F_R), sensible and latent heat (F_S and F_L), melting flux (F_{melt}), transmitted solar radiation, (I_R), and turbulent exchange with the underlying mixed layer ($F_{entrain}$). About 60% of the solar radiation (F_R) is absorbed as it passes through the lead, providing a source of heat for warming of the lead water and lateral ice melting. Sensible and latent heat fluxes are typically upward (cooling of the water) because the water temperature is usually higher than the air temperature. Loss of heat to the mixed layer is controlled mostly by turbulent mixing that is forced by wind driven currents in the lead and dynamic ice movement. During periods of weak winds and fresh water runoff into leads (as observed during the summertime SHEBA experiment), $F_{entrain}$ is reduced because of strong stratification and low turbulence levels. With these conditions, incoming solar radiation is not balanced by the combined fluxes, leading to an increase in the lead temperature. However, because ice melting rates are proportional to the difference between the freezing point of sea water and the water temperature, the melting flux, F_{melt}, increases and eventually balances the excess incoming radiation, arresting the increase in lead temperature.

[7] The timescales associated with lead heat flux balances are many days and cannot be simulated using the large-eddy simulation (LES) model applied here. Instead, we focus on short duration simulations that provide a measure of the flux balance without reaching equilibrium. For example, in one set of simulations we compare melting fluxes for different size leads, starting with an average lead heat content that is nearly in balance. We also examine how stronger winds act on an existing fresh layer to see how lateral fluxes are affected by changes in $F_{entrain}$. Because of the computational cost of our experiments, we cannot build a data set for establishing an improved parameterization. Our hope is that the work contained here will provide insight on how leads regulate lateral melting by trapping fresh water, which will eventually be used to motivate changes in current lead parameterization methods.

[8] The paper is organized as follows. In section two, we briefly describe the model and initial conditions used in the study. Model experiments and results are presented in section 3 for a range of lead sizes and wind forcing parameters. Results are discussed in Section 4 along with suggestions for lead parameterizations and conclusions.

2. Model and Initial Conditions

2.1. Model Description

[9] Simulations were performed using an extended version of the coupled ice-ocean LES model described previously by *Skyllingstad and Denbo* [2001] and *Skyllingstad et al.* [2003]. Briefly, the model is based on the filtered, nonhydrostatic Navier Stokes equations described in *Tripoli* [1992] with ice represented as a slab with a linear temperature profile [*Maykut*, 1978]. Exchanges of salt and heat between the ice and ocean are parameterized using transfer coefficients following *McPhee et al.* [1987], with ice temperature set to the melting point at the ocean interface. Because of the relatively short duration of the simulations (4 hours), ice properties (e.g., mass, salinity) were held constant. Ice melting along the lead edge and under the ice pack resulted in a fresh water flux, however snow and ice surface melt water runoff were only considered in experiments examining the initial establishment of the lead fresh layer.

[10] In the original model, fluxes between the ice and ocean were limited to the vertical direction between the seawater and the bottom, horizontal ice surface. Variations in the ice thickness did not exceed Δz between adjacent grid points. Here, the basic model was altered by allowing for lateral melting at the edge of the ice when the ice thickness change exceeds a full vertical grid increment. As a simplification, we considered only a vertical ice edge with depth variations discretized to full Δz increments and ignored the flux of heat between the ice edge and the ice interior. Fluxes between the ice and ocean on vertical surfaces were

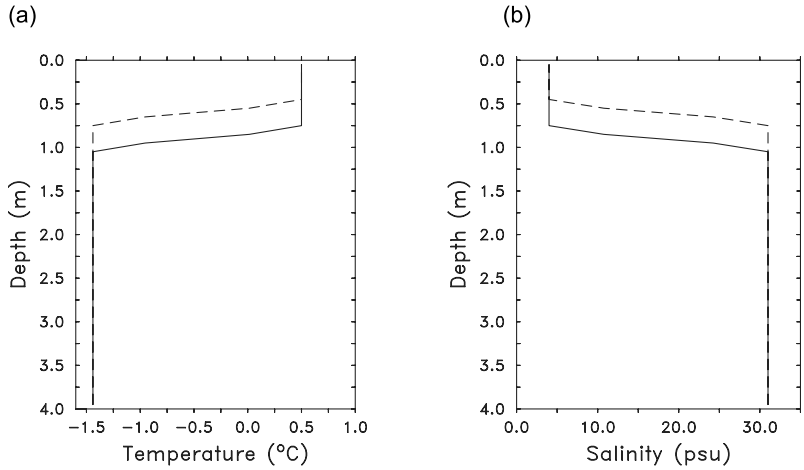

Figure 2. Initial profiles of (a) potential temperature and (b) salinity for the 1.0 m (solid lines) and 0.5 m (dashed lines) fresh layer cases. The fresh layer temperature is from case C24_1.

modeled using the same coefficients as the horizontal ice bottom, but with a friction velocity estimated from both the vertical and horizontal flow speeds. For example, for an ice edge parallel to the *x*-*z* plane, the local friction velocity or momentum exchange was defined as

$$\left\langle u_i'' u_k'' \right\rangle = C_D \Delta u_i |\Delta u_i| = u_*^2, \tag{1}$$

where

$$C_D = \left[\frac{\kappa}{\ln\left(\delta x / z_0 \right)} \right]^2, \qquad \Delta u_i = \sqrt{\left(\bar{w}_{i,k}^2 + \bar{v}_{i,k}^2 \right)},$$

z_0 is the ice aerodynamic roughness set to 0.005 m [*McPhee*, 2002], δx is set to $1/2\Delta x$ denoting the distance from the ice edge to the sea water grid cell center, and *i*,*k* represent the indices of the sea water grid cell adjacent to the lateral ice edge. Overbars on the velocity variables denote averaging from the Arakawa C staggered grid configuration to the grid cell center. Grid dimensions were set to 44.8 m in the *x* and *y* directions and 4.0 m in the vertical direction with spacing of 1 m.

2.2. Initial Conditions and Simulation Parameters

[11] Model initial conditions were set using idealized versions of temperature and salinity profiles taken from lead conductivity, temperature, depth (CTD) measurements reported by Pegau and Paulson (submitted manuscript, 2005). Our goal was to initialize a lead temperature that yielded a steady ice melting flux. At first, we planned to use a single profile representing conditions in early summer, and conduct simulations until reaching a steady ice melting flux where the lead water temperature was almost constant. However, this strategy proved to be unfeasible because of the large time period required to reach thermal equilibrium. For example, if the model temperature was initialized too warm, then ice melting fluxes would start out large and have a gradual downward trend as the water cooled. To get around this problem, we conducted a number of short, test simulations designed to select a lead temperature that would yield steady melting fluxes. A more detailed explanation of this procedure is provided in the results section.

[12] In most of the cases presented here, the fresh water layer in the lead was set to a depth of ~1 m as shown in Figure 2. We also investigated a limited number of shallow fresh layer cases (0.5 m depth) to see how fluxes differed from the deeper fresh layer. Simulations were started at rest, with forcing driven by surface wind stress on the open lead surface or by ice motion. Tests with ice motion were examined and found to be very similar to stationary ice cases, so we did not consider cases with ice motion. Ice motion with very large leads (~500 m) might have a greater influence, however, here our focus was on small leads as were observed during SHEBA.

[13] Some of the basic questions we wanted to answer with the LES model included assessing the effect of lead size, fresh layer thickness, and wind forcing. Ideally, we would like to have considered a lead similar in scale and shape to the SHEBA observations, for example, Sarah's Lake (see Pegau and Paulson, submitted manuscript, 2005), which was hundreds of meters in scale and had a complex shape. However, computational cost considerations forced us to limit our experiments to much smaller leads with a simple shape, for example a square. Use of linear lead edges also simplified our calculations of lead edge characteristics. In this paper, we consider two lead sizes, 16 × 16 m and 24 × 24 m, and two fresh water thicknesses as shown in Figure 2, along with a completely uniform initial condition. Forcing and initial conditions are summarized in Table 1, providing the lead size, wind stress, and initial fresh layer temperature for each case. For most of the experiments, the fresh layer depth was set to 1 m, although a limited set of experiments were conducted with a shallow, 0.5 m fresh layer. Weak wind cases represented conditions that existed most of July during the SHEBA experiment. Stronger wind cases were designed to see if increased wind stress can actively mix the fresh layer contained within small leads and place a timescale on total mix out of a fresh capped lead. Solar heating and sensible plus latent heat flux were

Table 1. Parameter Values for Lead Size, Fresh Layer Thickness, and Wind Stress

Experiment	Lead Size, m^2	Wind Stress, N m^{-2}	Fresh Layer Temperature, °C
C24_02U	24	0.02	no fresh layer
C24_1U	24	0.1	no fresh layer
C24_02C	24	0.02	1.0
C24_1C	24	0.1	1.0
C24_02	24	0.02	2.5
C24_1	24	0.1	0.5
C16_02	16	0.02	2.0
C16_1	16	0.1	0.0
C36_02	36	0.02	3.0
C24_05	24	0.05	2.0
C24_07	24	0.07	1.0

set to 240 and -30 W m^{-2}, respectively, with the vertical transmission of visible radiation prescribed according to Pegau and Paulson (submitted manuscript, 2005).

3. Results

3.1. Initial Lead Stratification Setup

[14] Estimates of ice edge melting rates can be made using simple geometric relationships between the ice edge area and total lead area. For example, under ideal conditions, input heat flux at the top and bottom of a square lead is proportional to the area of the lead, L^2, where L is the width of the square lead. Conservation of energy requires that the difference between the downward flux at the top and bottom of the lead must equal the sum of the lead water heat content change and the lateral melt flux. Using this conservation principle, we can formulate a lead heat budget as

$$L^2\left(F_{\text{top}} - F_{\text{bottom}}\right) = 4LhF_{\text{melt}} + C_p\rho hL^2 DT/Dt, \qquad (2)$$

where $F_{\text{top}} = F_{\text{R}} + F_{\text{L}} + F_{\text{S}}$, $F_{\text{bottom}} = F_{\text{entrain}} + I_{\text{R}}$, h is the ice thickness along the lead edge and DT/Dt is the total change in heat content or heat storage of the lead water. We can imagine limiting cases using (2), for example, if the lead is isolated from the rest of the ocean mixed layer so that $F_{\text{entrain}} = 0$ and the lead temperature is in equilibrium ($DT/Dt = 0.0$), then

$$F_{\text{melt}} = \left(F_{\text{top}} - I_R\right)L/(4h). \qquad (3)$$

This limit indicates that the larger the lead, the greater the edge melting, assuming that the average lead water temperature does not change and water is not exchanged between the lead and the rest of the ocean. However, most current parameterizations of lateral melting assume that the lead water has properties matching the underlying ocean; basically ignoring the effects of trapping within the lead [*Bitz et al.*, 2001; *Holland et al.*, 1997]. Data from SHEBA show that this assumption is probably wrong during much of the summer melt season when fresh water is trapped in leads. What we do not know is how wind stirring and ice motion affects the formation of stable layers in leads and if stratification can be prevented by frequent summer wind events. Simulations presented here examine how winds affect lead stratification and control the flux balance of the lead water.

[15] We begin our discussion by examining the initial warming of a lead starting with temperature and salinity profiles that are well mixed throughout the lead and upper ocean. These conditions are representative of the early summer when significant melting has set in and thin ice has melted through to form the first significant leads of the summer. We consider both weak wind and strong wind scenarios, cases C24_02U and C24_1U, respectively (Table 1) with constant water properties of $T = -1.44$ and $S = 31$. On the basis of the SHEBA observations, leads developed a stratified structure in the early summer because of solar heating and fresh water input from the surrounding surface melt. Although we suspect that stratification from melt water dominates the lead structure, we wanted to determine if solar heating alone could stratify a lead and enhance lateral melting.

[16] Our analysis begins with a plot of the significant heat budget terms within the simulated lead. Fluxes shown throughout the paper are calculated based on the average heat balance for a unit column of water 1.3 m deep. The averaging depth was chosen so that heat budget terms would not include the effects of ice bottom melt, which are evident below ~1.4 m. Terms in the heat budget plots are the total flux or storage ($C_p\rho hDT/Dt$), entrainment flux (F_{entrain}), and the scaled wall flux ($F_{\text{melt}}4h/L$). Remaining terms in the heat balance, namely, $F_{\text{R}} + F_{\text{S}} + F_{\text{L}} - I_{\text{R}}$ equaled a constant 116.4 W m^{-2} in all of the simulations.

[17] Results from a 4 hour simulation with weak wind forcing (Figure 3) and no surface melt water flux show that the local lead heat balance is dominated by entrainment mixing, with the average lateral heat loss being relatively insignificant at around 15 W m^{-2} (melting fluxes at the ice edge are $L/4h$ or 4 times this value). Lead temperature is increasing slightly as shown by the positive value of the storage term. However, as the horizontally average temperature from hour 4 and 0 demonstrates (not shown), the change is relatively uniform throughout the water column extending below the lead and therefore has a negligible effect on the stratification. Influx of fresh water from melting along the lead edge is minor with this case and has little influence on the lead stratification. A similar result is obtained with the stronger wind scenario, suggesting that only very calm wind conditions can lead to significant

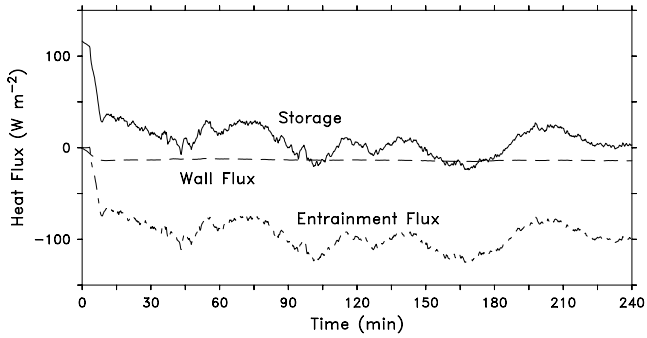

Figure 3. Time series plots of the storage, wall melt flux (F_{melt}), and entrainment flux (F_{entrain}) from a 24 m square lead initialized with uniform temperature and salinity (case C24_02U). Lateral melting (as indicated by the wall flux) uses only a small fraction of the incoming solar radiation.

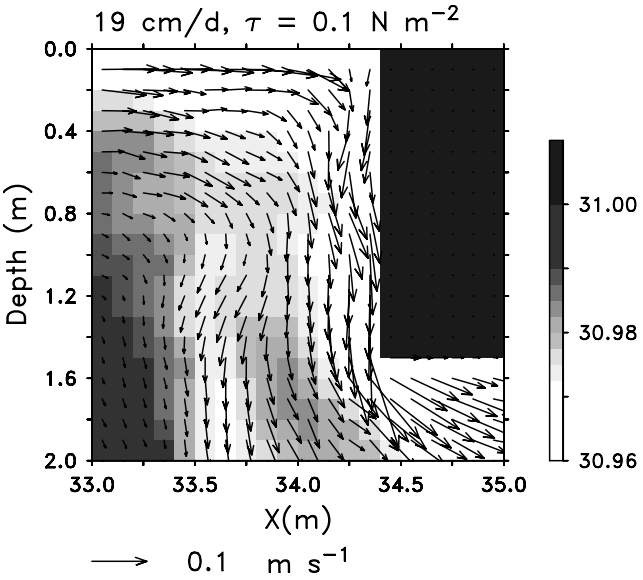

Figure 4. Vertical cross section showing salinity and current vectors from the strong wind case (C24_1U) with a surface salt flux of 19 cm d^{-1}. The plot is taken from the center of the lead at y = 22.4 m.

warming of the lead water in the absence of a fresh water flux. On the basis of this result, we conclude that melt water plays a dominant role in stratifying summer leads.

[18] During the SHEBA field experiment, surface melting started around the beginning of June and extended until mid-August [*Eicken et al.*, 2002; *Perovich et al.*, 2003]. Average surface melt rates ranged between 1 and 4 cm d^{-1} over the surveyed ice area. Analysis of the lead fresh water depth growth rate made by Pegau and Paulson (submitted manuscript, 2005) indicated a fresh water flux of ~6.5 cm d^{-1} over the 20 day period between 29 June and 19 July 1998. Assuming a lead fraction of 5% [*Perovich et al.*, 2002] and an average melt rate of 1.5 cm d^{-1} indicates that only about 1% of the available melt water ends up in leads, with the remaining melt water trapped in ponds on the ice surface and beneath the ice cover [*Eicken et al.*, 2002].

[19] In our next set of experiments, we test how the addition of fresh water affects lead stratification. Two fresh water flux cases are considered; one at 19 cm d^{-1} and a second with 9.5 cm d^{-1}. These two cases represent lead fresh water depth changes that were observed for short periods in early July 1998 by Pegau and Paulson (submitted manuscript, 2005). Simulations with fresh water flux are started after the model has simulated 4 hours with weak wind forcing (case C24_02U) and 1 hour with strong wind forcing (case C24_1U), and is near steady state.

[20] Results from the strong wind case showing cross sections of salinity and current vectors are presented in Figure 4 for the 19 cm d^{-1} fresh water flux. As shown by Figure 4, water with reduced salinity is forced along the lead edge and under the ice and does not collect in the lead. Lowering of the lead salinity in this case does not produce enough stratification to counteract the motion of the water generated by the surface winds. With the low-wind forcing, a very different result is produced as shown in Figure 5 for the 19 cm d^{-1} and 9.5 cm d^{-1} flux cases. Fresh water in these two cases does not have enough downward momentum to overcome the stratification at the lead edge and is consequently trapped in the lead. Plots of the heat budget for these two cases are shown in Figure 6, representing the 4 hour period after the salt flux is introduced. Overall, the two cases display similar behavior, with a rapid decrease in entrainment flux after the introduction of the fresh water flux, followed by steady conditions with most of the incoming solar heat going toward warming the lead water as shown by the large storage term. Scaled lateral wall fluxes in both cases are relatively small (~15 W m^{-2}) because of the cold lead water temperatures.

[21] Given a long enough time without significant wind forcing, the combination of fresh water flux and solar

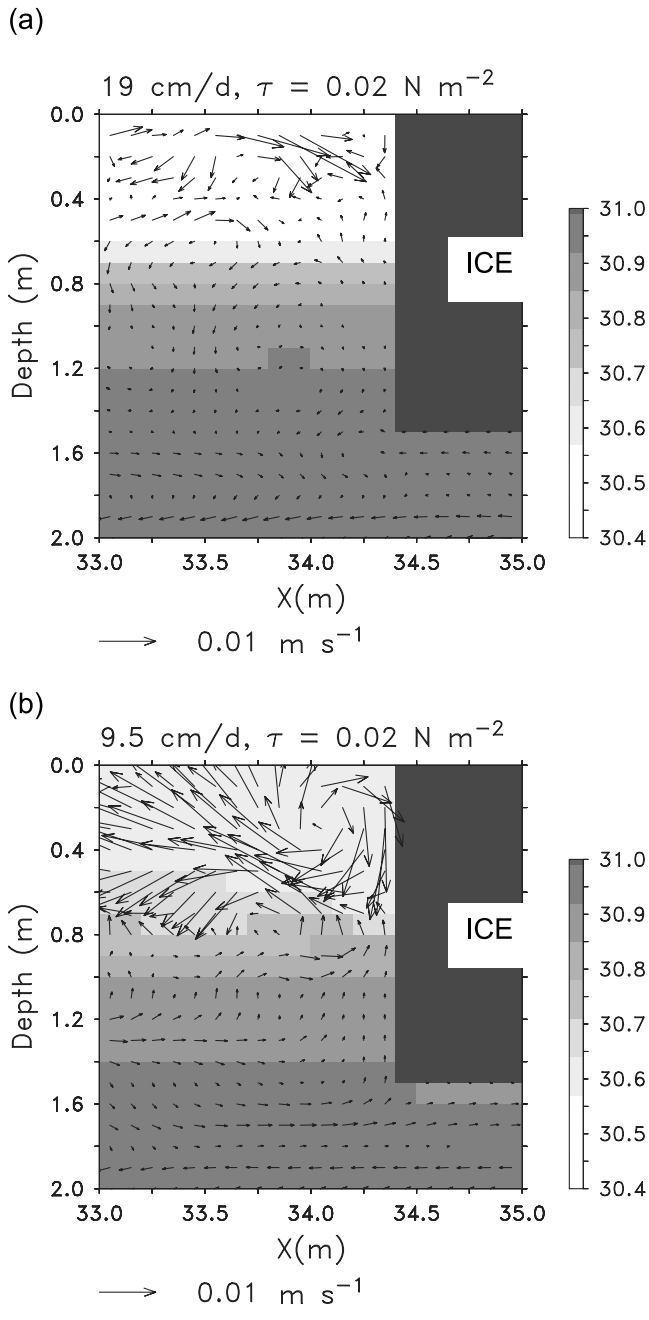

Figure 5. Same as Figure 5, but for the low-wind case (C24_02U) and fluxes of (a) 19 cm d^{-1} and (b) 9.5 cm d^{-1}.

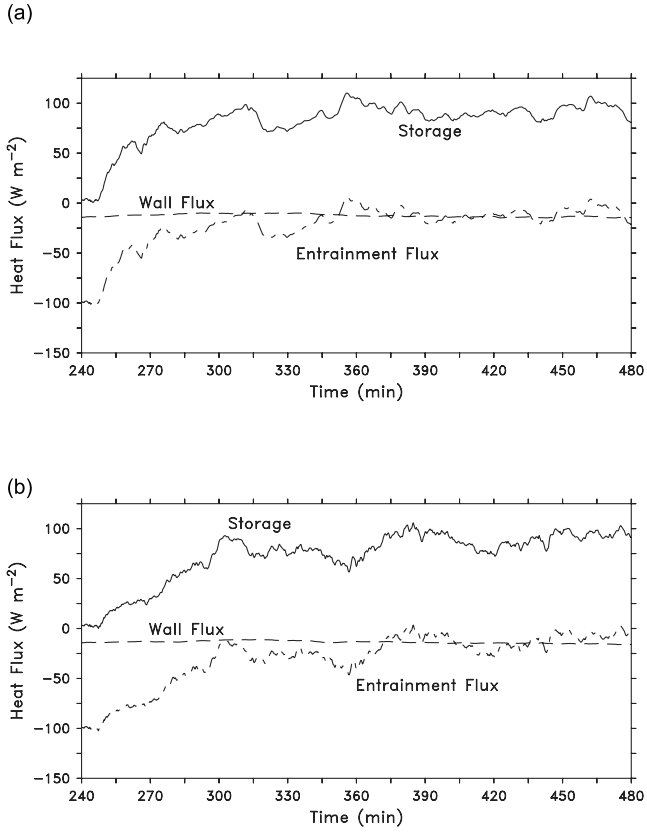

Figure 6. Same as Figure 4, but for a lead salt flux of (a) 19 cm d^{-1} and (b) 9.5 cm d^{-1}.

heating will result in a warm, fresh lead water system as was observed during SHEBA. This process takes many days and is computationally expensive to simulate with LES. In addition, the resolution of the LES model is insufficient to duplicate the very sharp salinity gradient measured in leads. The model cannot simulate these sharp gradients because of the implicit mixing that occurs over the top grid cell when decreasing the water salinity. Salinity gradients in the model are always limited by the grid resolution, whereas observations show very strong gradients over distances of a few centimeters. Finally, it is possible that cooling of the fresher lead water by colder, saltier water beneath the fresh layer can cause freezing of frazil ice particles at the base of the fresh layer. Salt is rejected as frazil freezes and the particles rise and melt, which effectively desalinizes the vertical water column. This process is not accounted for in the model and would probably be incorrectly modeled in any case unless much better resolution were applied so that small-scale mixing associated with the lead halocline could be accurately simulated. Our strategy to get around these issues was to initialize a fresh layer structure similar to the observed SHEBA cases as shown in Figure 2.

3.2. Fresh Layer Evolution

[22] Our next set of experiments focuses on the evolution of a warm, fresh layer in response to differing surface wind stress and lead sizes. For our first experiment, we examine the effects of wind stress variation for a 1 m deep fresh layer having an initial temperature of 1°C (see Figure 2) for a 24-m-wide lead. We again applied the weak and strong wind forcing as defined in Table 1 (cases C24_1C and C24_02C) and conducted simulations for 4 hours. Plots of the heat budget for these two cases (Figure 7) indicate the importance of wind-generated stirring on the heat balance. In both cases, the storage term is positive indicating that the lead is gaining thermal energy. Differences between the two cases are in the strength of the individual terms; in the weak wind case, storage is roughly double the strong wind value, whereas both entrainment and wall flux in the strong wind case have larger magnitudes than the weak wind case. As plots of the average lead temperatures show (Figure 8), the net effect of these flux differences is fresh layer cooling in the strong wind case and warming in the weak wind case, even though the storage term in both cases is positive. In the strong wind case, fresh layer deepening offsets solar warming in the top ~1 m of the lead, resulting in cooling in the upper portion of the water column that is offset by relatively stronger warming below 1 m.

[23] Plots of the time-dependent average fresh layer temperature (not shown) suggest that each of the above cases would eventually reach a steady temperature, where incoming heat is roughly balanced by the wall flux and entrainment flux. Lead observations from SHEBA suggest that after the lead was capped by fresh water, temperatures became relatively steady at about 1.5°–2.0°C. Because of computational costs, we could not conduct simulations long enough to reach a steady lead temperature as was observed. Instead we used a trial and error method for selecting the initial fresh layer temperature. Depending on the wind speed

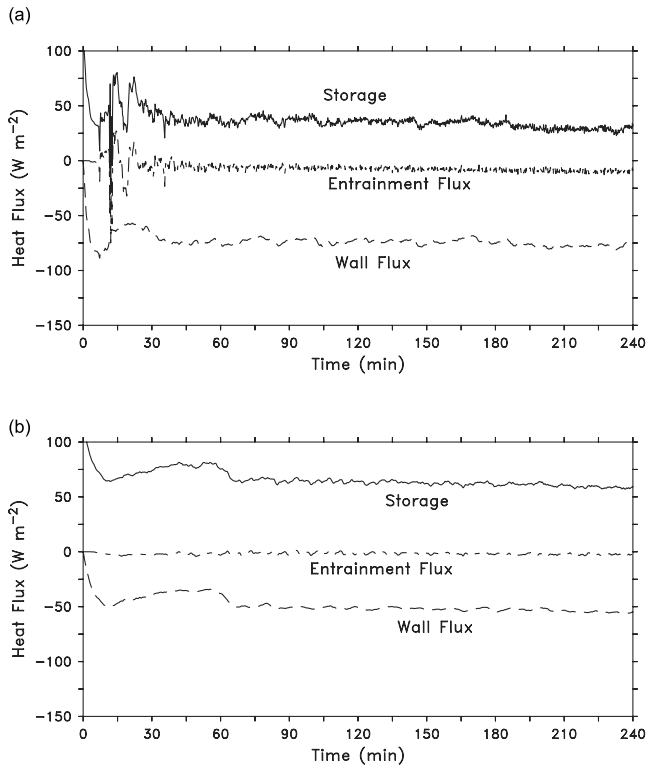

Figure 7. Heat balance terms for a 1 m fresh with initial temperature of 1°C, forced with wind stress of (a) 0.1 N m^{-2} and (b) 0.02 N m^{-2} (cases C24_1C and C24_02C, respectively). Fluxes are averaged over the top 1.3 m of the lead water.

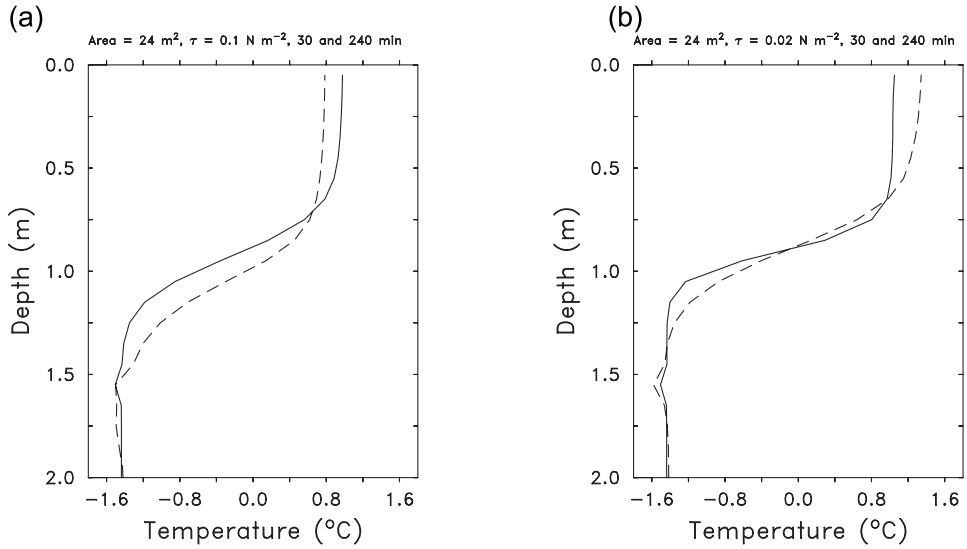

Figure 8. Horizontally averaged temperature for cases winds stress of (a) 0.1 N m^{-2} (case C24_1) and (b) 0.02 N m^{-2} (case C24_02). Plots are at 30 min (solid lines) and 240 min (dashed lines).

and lead size, the fresh layer temperature was set to a value yielding a near steady surface value over time. Initial fresh layer temperature values are shown in Table 1 for each of the experiments. Plots of the 1 m averaged temperature for the primary cases (Figure 9) show that the lead temperatures were relatively steady, indicating that our selection process was successful.

[24] In our first test with near-equilibrium conditions we wanted to examine how lead size affects lateral melting. As shown above in (3), if the fluxes at the top and bottom of the square lead are the same and storage of heat is minimal, then the difference in lateral melt flux should be equal to the ratio of the lead widths. Lateral melt flux in this context is F_{melt}; not to be confused with the scaled wall flux, $F_{\mathrm{melt}}4h/L$, used above in the lead heat budget calculations.

[25] Experiments were performed using two main lead sizes, 16 and 24 m, with a single additional experiment performed with a lead width of 36 m to see if increasing the lead size further changes the melt flux. Plots of the lateral heat flux (Figure 10) for the different lead sizes and wind stress values given in Table 1 show that, in general, lateral flux increases with increasing lead size, but not according to the simple steady state formula given in (3). This is most clearly shown by the strong wind cases which both have much weaker lateral melt flux indicating that solar radiation is warming the lead water. This makes sense because we had to decrease the fresh layer temperature to 0.0°C for the 16 m case and 0.5°C for the 24 m case to achieve a near steady state fresh layer temperature. The ratio of the 24 m and 16 m cases for strong winds is about 1.8, which is higher than predicted by (3) and is probably related to the more efficient lateral heat transport in the larger lead. Wind stress acting on the water surface of the large lead is able to generate stronger currents that move water more quickly from the center of the lead to the lead edge. Consequently, we see higher heat fluxes than expected for the larger lead case, although the change in heat flux with time is about the same in both cases.

[26] Melt fluxes from the low-wind cases show a much different behavior in comparison with the strong wind cases. With these cases, the ratio of the 24 m to 16 m is about 1.4, which is closer to the 1.5 predicted by (3). In addition, the melt flux is relatively steady over time, suggesting that incoming heat is being balanced by the lateral melt flux. We again had to use different initial fresh water temperatures

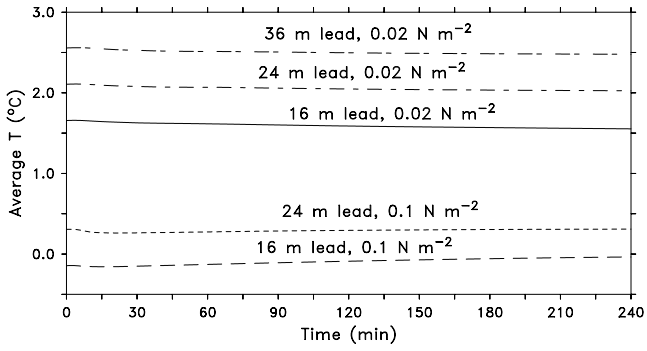

Figure 9. Vertically and horizontally averaged temperature (°C) for cases C16_02, C16_1, C24_02, C24_1, and C36_02. The vertical average is taken between the surface and 1 m depth.

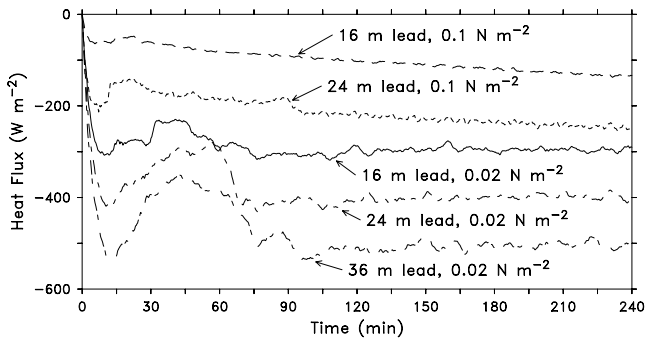

Figure 10. Average lateral heat flux from cases C16_1, C16_02, C24_02, C24_01, and C36_02.

(2.0°C and 2.5°C for the 16 m and 24 m leads, respectively) to approximate a steady state solution, indicating that as lead size increases, low-wind conditions will lead to warmer lead surface water temperature. Also, we note that in each case the wall flux magnitude oscillates slightly before settling into a steady rate. Changes in the initial melt rate are controlled local to the wall edge where ice melting cools the near ice water. Over time, currents generated by the surface wind force a lead circulation that transports this cooler near wall water away from the ice and ensures the cold water formed through melting does not collect at the ice edge. The duration of this initial oscillation is determined by the lead size and wind stress magnitude. Larger leads and smaller wind stress require more time for the cold melt water to transport away from the lateral ice edge.

[27] Examination of the total heat budget per unit volume for the 16 and 24 m cases (Figure 11) provides a more thorough description of the different behavior noted in the melt fluxes above. Overall, the wind stress value has the most significant effect on the heat budgets. With strong wind stress (Figures 11a and 11b), we note a consistent behavior between the two lead sizes, with the storage term beginning as the highest magnitude term and gradually decreasing over time. The reduction in the storage term is offset by a commensurate increase in the wall flux magnitude, indicating that as the lead water warms through solar radiation, the melting rate increases because of the greater heat content of the fresh layer. In contrast, the low-wind cases have a behavior more indicative of a steady state system. Storage in these cases is much lower in magnitude, settling to a value of $\sim$15 W m^{-2} in the 24 m case, and near zero in the 16 m case. Melting flux in the low-wind cases takes up almost all of the incoming heat, yielding a scenario similar to the SHEBA July situation where lead temperatures were steady and lateral melting flux balanced much of the incoming solar radiation.

[28] One puzzling aspect of the strong wind heat budget is the apparent warming indicated by the storage term, even though the surface temperature shows very little change over time. To explain this behavior, we present plots of the average vertical temperature profiles from the 24 m strong and weak wind cases at two different times (Figure 12). As Figure 12 shows, in the strong wind case, turbulent mixing generates a growing mixed layer with the heat flux generated by turbulent entrainment being offset almost exactly by excess solar heat flux in the upper fresh layer. Temperatures do drop slightly in the layer, but overall the greatest change is warming at $\sim$1 m depth as the mixed layer deepens. In comparison, the weak wind case displays mixing at the bottom of the warmer surface layer, as shown by a gradual decrease in the gradient at 1 m depth, but not much overall deepening. In the weak wind case, almost all the solar heat flux is used in lateral ice melt, so very little change occurs in the mean temperature profile aside from mixing from weak turbulence and molecular diffusion.

[29] A second set of fresh layer experiments was conducted to examine how fresh layer thickness affects the lead heat budget. In these experiments, we used the same fresh layer temperatures as in the previous cases, but with layer thickness initialized at 0.5 m instead of 1.0 m. Heat budget terms from these cases (Figure 13) are very similar to the 1 m deep fresh layer cases, especially for the strong wind stress experiments. In the weak wind cases, flux terms quickly reach a steady state, but show a large increase in the storage term to $\sim$40 W m^{-2} in comparison with a 0–

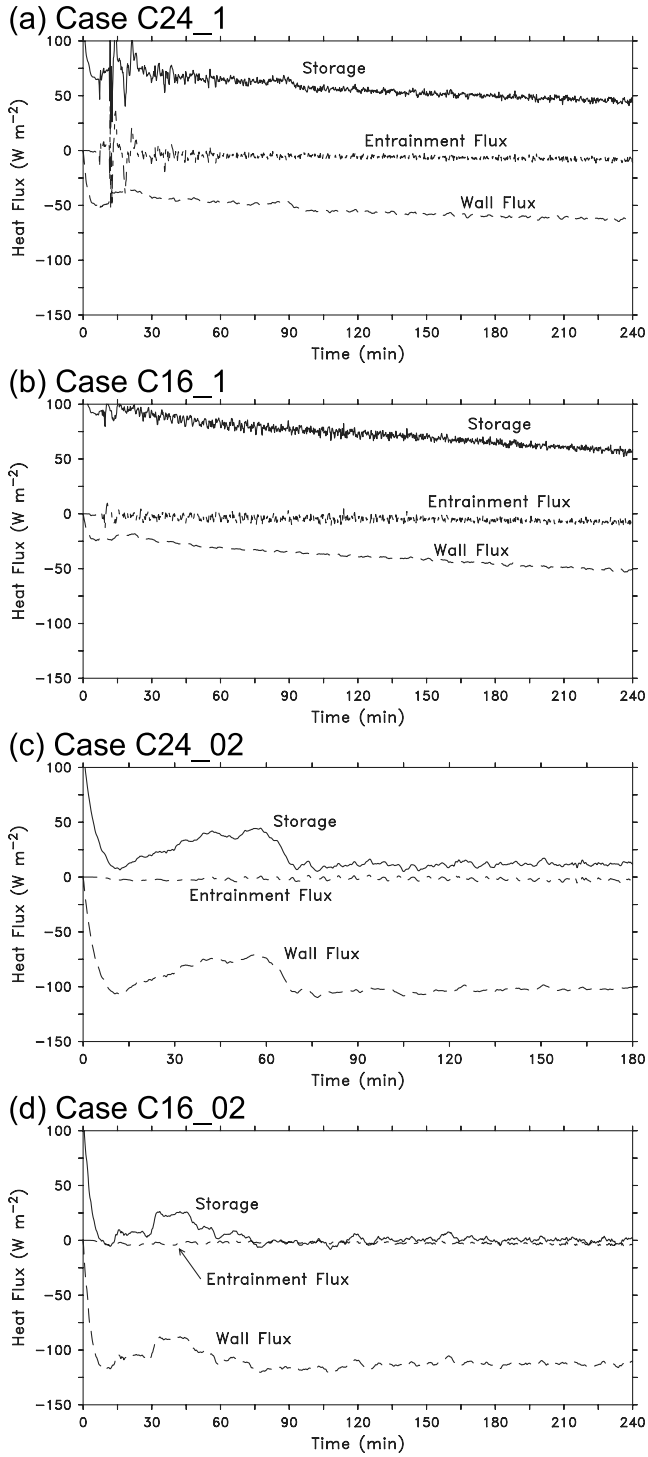

Figure 11. Time series plots of the storage, wall melt flux (F_{melt}), and entrainment flux ($F_{entrain}$) from cases with a wind stress of 0.1 N m^{-2} and lead width of (a) 24 m and (b) 16 m and from cases with a wind stress of 0.02 N m^{-2} and lead size of (c) 24 m and (d) 16 m. Initial fresh water depth in each case was 1 m.

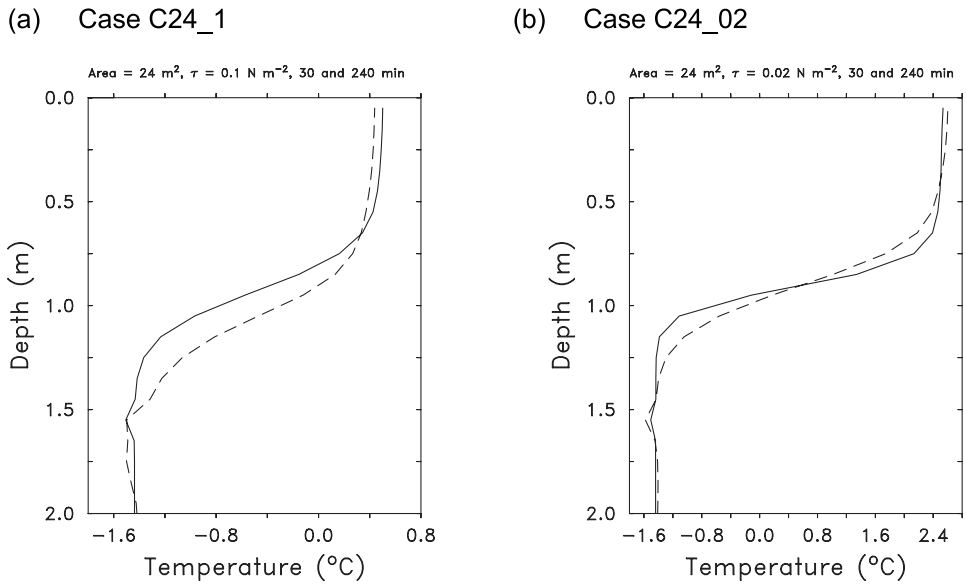

Figure 12. Vertical profiles of the horizontally averaged temperature from the (a) strong wind case (τ = 0.1 N m^{-2}) and (b) weak wind case (τ = 0.02 N m^{-2}). Profiles are from 30 (solid lines) and 240 (dashed lines) min in each case.

15 W m^{-2} storage for the 1 m cases. By reducing the depth of the warm, fresh layer in the weak wind case, we have decreased the volume of warm water in contact with the ice edge by about 50%. The net effect is greater heating in the new simulation as shown by the larger storage term. We do not see similar changes in the strong wind case because the water temperature is not warm enough in the fresh layer to weigh heavily on the heat budget.

[30] It is interesting to compare our model results with measurements taken by Pegau and Paulson (submitted manuscript, 2005). In their lead analysis, they estimated a lead perimeter of ~817 m and a lead area of ~12,000 m^2. These dimensions yield a area/perimeter ratio that is much different than the square lead assumed here. Small, narrow inlets and points greatly increase the perimeter area for actual leads. For example, a square lead with area of 12,000 m^3 would have a perimeter of about 400 m versus 817 m reported by Pegau and Paulson (submitted manuscript, 2005). Nevertheless, estimates of the observed scaled wall flux given by Paulson and Pegau ranged between 50 and 100 W m^{-2}, which are values similar to our results shown in Figure 11. Total average edge melting flux over the melt season was estimated at ~800 W m^{-2}, which is also consistent with our low-wind results shown in Figure 10 when lead size and perimeter are taken into consideration. This can be shown by computing the ratio of the area/perimeter for the observed and modeled leads. For the 36 m simulated lead, area/perimeter = 36/4 = 9, whereas the observed lead area/perimeter = 12,000/817 = ~15. Multiplying the observed melting flux (~800 W m^{-2}) by the ratio of these two parameters yields a melting flux of ~500 W m^{-2}, which is similar to the simulation result in Figure 10 for the 36 m lead.

3.3. Lead Circulation

[31] Heat transport from the center of the lead to the ice edge can be accomplished through two main processes. The first transport process is through small-scale turbulence; if the lead water is turbulent, then eddies will transport heat laterally based on the rate at which eddies can exchange scalar quantities in the horizontal direction. The second, much more efficient way to transfer heat from the center is through horizontal circulation currents that are forced by the wind and contained within the lead boundaries. Examples of lead circulations are shown in Figure 14 from the strong and weak wind fresh layer cases (C24_1 and C24_02) and the strong wind uniform case (C24_1U). For the fresh layer cases, examination of Figure 14 shows a similar flow behavior for both wind stress values with the strongest downwind currents near the sides of the lead and currents opposing the winds in the middle of the lead. The strong wind stress case indicates current speeds that are about double the weak wind case, which is consistent with a near doubling of the wind stress friction velocity. Without fresh water trapping, the current structure takes on a much different appearance as shown by the uniform initial condition case in Figure 14c. Here, the velocity increases steadily as the wind acts on the lead surface, with vigorous small-scale turbulent eddies developing in the downstream half of the lead. We recall that the vertical current structure for this case (see Figure 4) shows surface lead water being forced down along the down wind lead edge and out along the ice bottom. Figure 14 completes this picture by showing how the surface water picks up momentum from the surface stress before sinking along the lead sides and downwind ice edge.

[32] Wind forced currents have a large impact on where ice melts most rapidly on the lead edge as shown by plots of lateral ice edge melt flux (Figure 15) and current velocity for the weak wind case. As a first guess, one might think that ice edge melting would be maximized at the downwind edge of the ice where water warmed by the sun in the middle of the lead impacts the lead edge. However, the weak wind simulations show that the edge regions with

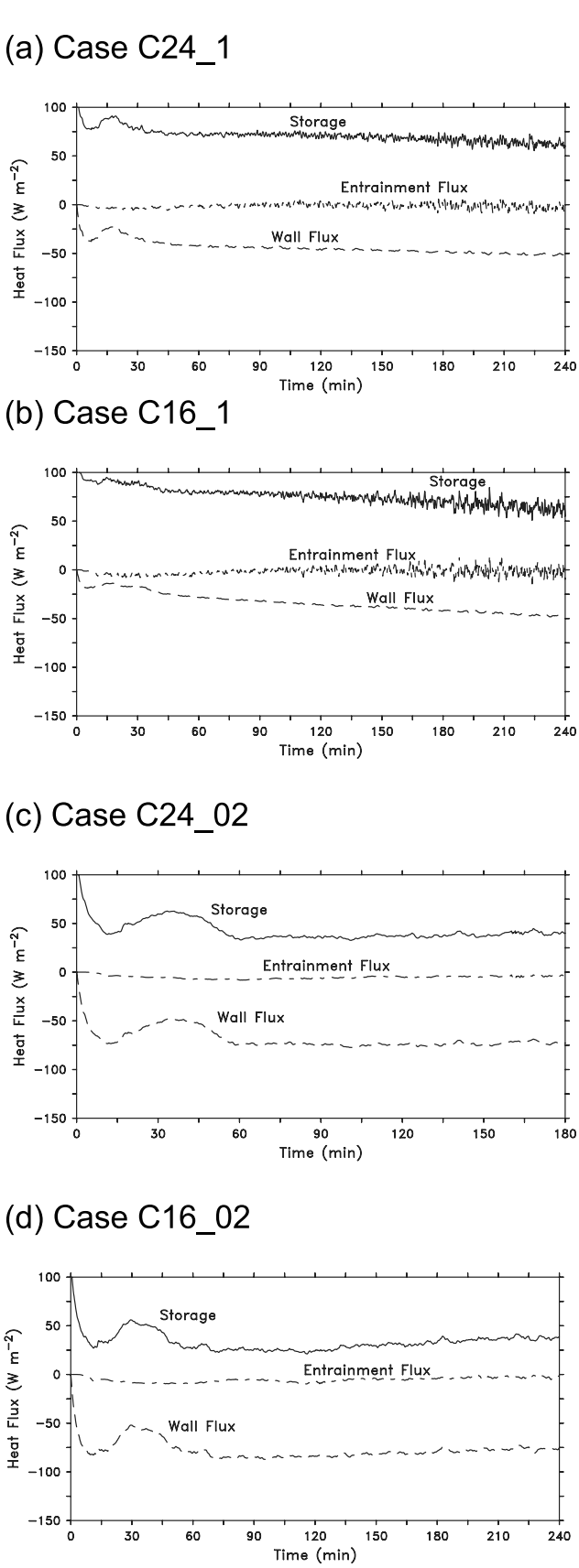

Figure 13. Same as Figure 12, but with initial fresh layer depth of 0.5 m.

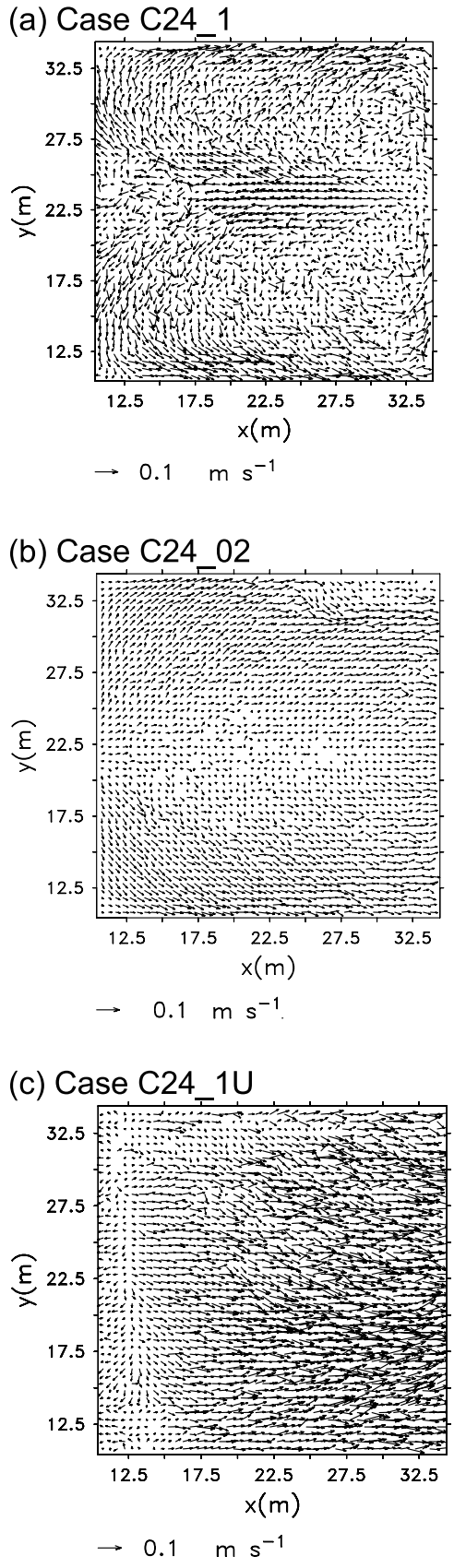

Figure 14. Horizontal cross section plots of velocity vectors at 0.4 m depth for the 1 m fresh layer cases with (a) wind stress of 0.1 N m^{-2}, (b) wind stress of 0.02 N m^{-2}, and for (c) the uniform initial condition case with 0.1 N m^{-2}.

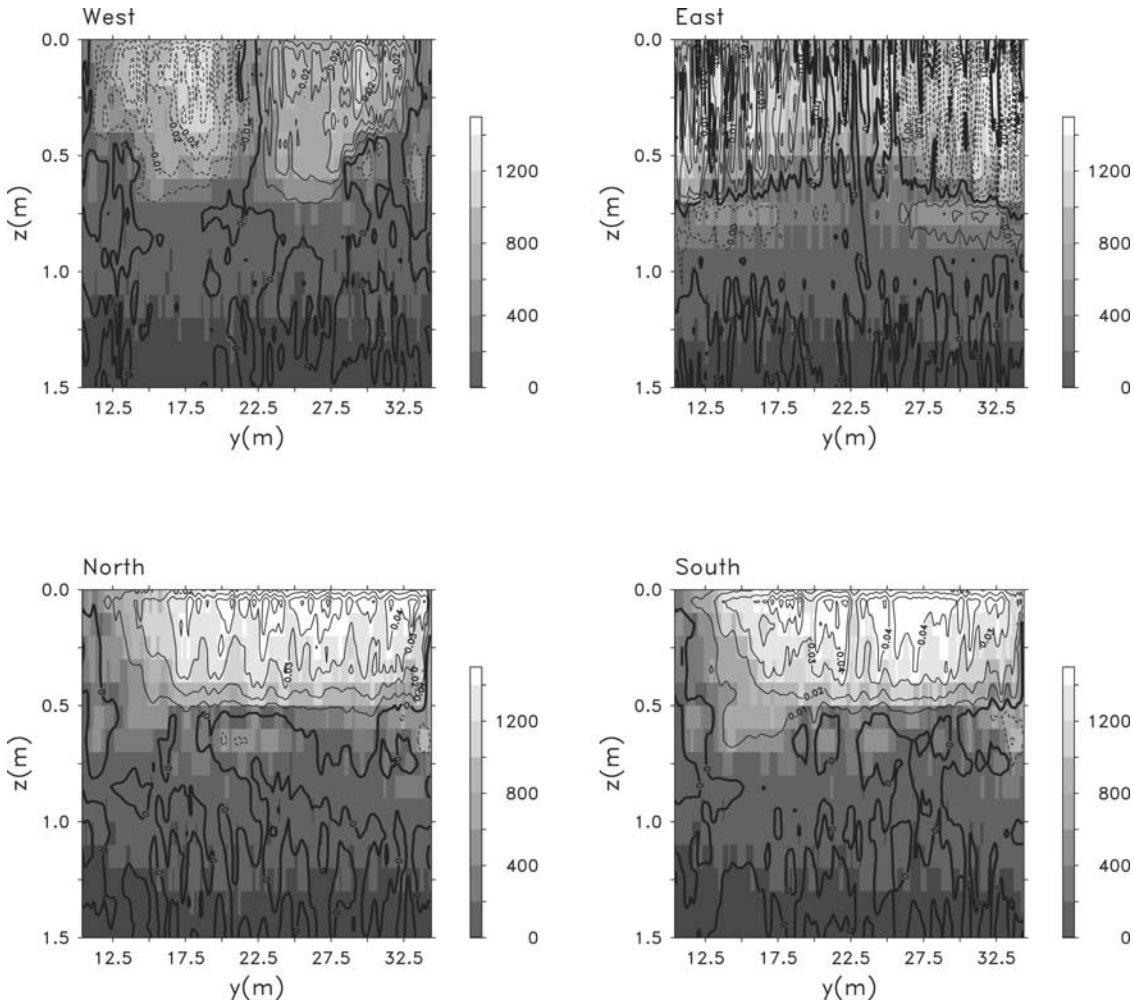

Figure 15. Vertical cross sections of the ice edge heat flux (W m^{-2}) and tangent current velocity (m s^{-1}) taken from the 24 m lead with a wind stress of 0.02 N m^{-2} after 4 hours (case C24_02). Each plot represents one face of the square lead with compass directions in the north-south direction corresponding to the y axis (with the u velocity component) and east-west corresponding to the x axis (with the v velocity component).

the strongest current velocities tend to have the highest melt rates. Here, current velocities are a maximum on the north and south edges where the flow is in the direction of the wind stress. Flow at the east and west ends of the lead is dominated by convergence and divergence, and corresponding weaker currents. Overall, the differences in current speed translate into flux differences of about 400 W m^{-2}. A similar correspondence between current speed and melting rate is produced in the strong wind case (not shown). However, the colder water required for steady state in the strong wind case dominates over the current speed in determining the melting rates. Much of the variability in the currents can be attributed to the idealized lead shape. Natural lead shapes are quite variable and would most likely have complicated edge shapes that would generate much different current structures and edge melting rates.

3.4. Effects of Changing Wind Stress

[33] Experiments shown so far considered only two wind stress values, which produced very different fresh layer behavior. The stronger wind stress case required a much cooler initial temperature than the weak wind case in order to maintain thermal equilibrium, which gave a lower overall melting rate. Larger current velocities with the strong wind case greatly increased the transport of heat to the ice edge, which over time cooled the water so much that the melting rate decreased. In addition, the stronger currents also generated more entrainment mixing, which caused a gradual deepening of the fresh layer and further heat loss. Deepening was not evident in the weak wind stress case during the simulation because of the much lower circulation current speeds.

[34] To help define when the wind stress becomes a dominant factor controlling the heat balance, we examined two intermediate cases with a lead size of 24 m and wind stress values of 0.05 and 0.07 N m^{-2}. As plots of the average lateral heat flux show (Figure 16), doubling the wind stress from 0.02 to 0.05 N m^{-2} increases the lateral melting rates for the 24 m lead rather than causing a decrease as shown with 0.1 N m^{-2} case. The difference between the 0.1 and 0.05 N m^{-2} cases is the strength of the

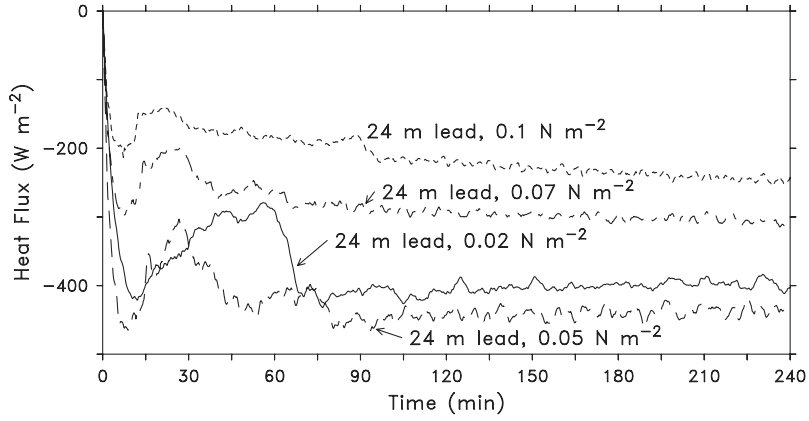

Figure 16. Average lateral heat flux for wind stress values ranging from 0.02 to 0.1 N m^{-2} for a 24 m lead. The average is performed on the ice edge perimeter around the lead.

fresh layer entrainment and the resulting water temperature decrease. Increasing the wind stress slightly to 0.07 N m^{-2}, however, produces a large change in the wall flux indicating that the increased circulation is affecting entrainment rate at the fresh layer bottom. In the 0.07 and 0.1 N m^{-2} cases, heat flux associated with deepening of the fresh layer balances a large portion of the incoming solar radiation, which greatly reduces the average water temperature and lateral melting.

4. Discussion and Conclusions

[35] Throughout this study, circulations were forced by prescribing a wind stress over the lead surface. We did not attempt to simulate the growth of surface waves, wave generated currents, or fetch depend stress that would exist in actual leads. To make sure that our model estimates are at least in the right ballpark with regard to actual wind driven currents, we compare our results with wave tank experiments reported by *Cheung and Street* [1988]. In these experiments, *Cheung and Street* [1988] measured wind and wave parameters for wind generated waves over a fetch of ~13 m and wind speeds ranging from 1.5 to 13.1 m s^{-1}. Results from these experiments corresponding to our idealized wind stress are shown in Table 2 for a range of wind speeds. Overall, the current velocities measured by *Cheung and Street* [1988] are about 2 times greater than the lead velocities corresponding to our prescribed wind stress. For example, for the strong wind stress case (C24_1), average surface lead currents are about 0.06 m s^{-1}, versus 0.14 m s^{-1} for the 0.12 N m^{-2} wave tank case given in Table 2. We note, however, that in our lead experiments the water motion was restricted by the closed lead causing flow recirculation. It is not clear if the wave channel would experience the same flow configuration.

[36] If we assume that the tank measured relationship between wind and wind stress is accurate, then the range of wind speeds examined in this study would fall between ~3 and 6 m s^{-1}, which are values similar to wind measurements taken during the summer SHEBA field program (adjusting for anemometer height only adds about 0.5 m s^{-1}). In fact, as shown by Pegau and Paulson (submitted manuscript, 2005), during the month of June when the fresh layer was thin, a number of wind events with velocities of 6–7 m s^{-1} apparently caused the newly formed fresh layer to weaken or entirely mix out (for example, around 1 July). As our simulations show, a fresh layer did not form when wind stress values of 0.1 N m^{-2} were applied. Lead behavior during SHEBA was similar in early summer when deepening fresh layers were destroyed by wind events. After 8 July the winds were rarely above 5 m s^{-1}, corresponding to wind stress values of less than 0.05 N m^{-2}, and the fresh layer deepened until filling the lead. In our experiments with fully turbulent fresh layers, wind stress values of 0.05 and below did not force strong deepening of the fresh layer through entrainment. For example, increasing the wind stress from 0.02 to 0.05 N m^{-2} caused cooling of the fresh layer through greater heat transport and lateral edge melt, but heat loss through entrainment was not greatly increased. In contrast, strong wind forcing caused the fresh layer to cool and deepen, so much so that the lateral melt rate decreased, even though the currents were stronger near the ice edge.

[37] Our simulations show that representing lead growth through lateral melting in coupled ocean/ice models requires more information than just knowing the bulk mixed layer properties. If we assume that the water in leads has the same properties as the ocean mixed layer under the ice, then melting rates will be greatly underestimated during periods of winds less than ~5 m s^{-1}. For example, in the case of a 24 m lead, melting heat fluxes with a 1 m fresh layer averaged ~400–450 W m^{-2} with light winds. Without the fresh layer, average melting fluxes for the same conditions were ~50–60 W m^{-2}. Lead observations taken during SHEBA support this result showing lateral melt rates that averaged ~800 W m^{-2} when winds were relatively weak.

[38] Results from the simulations also suggest that a key parameter for describing leads is the ratio between the lead

Table 2. Estimates of Wind Stress and Eulerian Current Speed for a 35 m Long Wave Channel for Various Wind Speeds[a]

Wind Speed, m s^{-1}	Wind Stress, N m^{-2}	Current Speed, m s^{-1}
2.6	0.012	0.07
3.2	0.024	0.07
4.7	0.052	0.09
6.7	0.128	0.14

[a]Taken from *Cheung and Street* [1988].

area, A, and the lead perimeter, P, or A/P. For the simulated square leads presented here, $A/P = L/4$, which gives a ratio of 25 for a 10,000 m^2 lead. In contrast, the 12,000 m^2 lead measured by Pegau and Paulson (submitted manuscript, 2004), had an effective $A/P = \sim 15$, because of large variations in the lead edge shape (inlets and points). The net effect of decreased A/P is more edge melting, resulting in lower lead temperatures for a given solar energy input. The lower A/P ratio of observed leads suggests that our results underestimate lateral melting for a given lead area. However, it may be possible to compensate for this difference by calibrating our results using estimates of A/P from ongoing analysis of aerial ice surveys from SHEBA and from future field experiments.

[39] A number of improvements could be included in current lead parameterizations based on the results of this study. At a minimum, parameterizations need some method for including the effects of fresh water trapping. One possible simple scheme could develop a fresh layer whenever the winds dropped below $\sim 7-8$ m s^{-1} for a prescribed period of time (e.g., roughly 4–5 days) and when atmospheric conditions (i.e., surface temperature, cloud cover) predict surface melting. Fresh layer growth could be estimated by assuming that 1% of the surface melt water enters leads and by using the lead fraction to calculate the incremental fresh layer growth. Observed wind speeds from SHEBA indicate that there was almost always a background wind stress of $\sim 0.01-0.02$ N m^{-2}, suggesting that lateral melt rates could be set to values calculated in this paper for low-wind conditions (with adjustments for differing P/A in naturally occurring leads), and applied over the predicted fresh layer depth. If winds increased to values greater than ~ 8 m s^{-1} for more than a few days, then the fresh layer would be mixed with the rest of the boundary layer by assuming a heat and salinity flux equivalent to adding the total fresh layer volume of water. For low winds, lateral melting rates in the model would be set to the total solar radiation absorbed in the fresh layer. As our experiments show, melting rates remain high until the fresh layer begins to deepen from entrainment. Increasing winds generate more cooling by transporting heat more efficiently to the lead edge. Nevertheless, the total available heat is still limited by the incoming radiation as long as the entrainment flux is small. Therefore as a first approximation, the fresh layer salinity and temperature could be ignored. However, including a simple bulk model for the fresh layer would probably yield more accurate results, but at the cost of maintaining more variables associated with the lead water.

[40] Although lateral melting is greatly increased when leads contain a fresh layer, it is not clear if the change in lead size from this effect is large enough to cause much greater ice melting through the ice-albedo feedback. Using the SHEBA field data, *Perovich et al.* [2002] show that during the July period of strong warming when leads were capped with a fresh layer, the average lead fraction stayed relatively constant at about 0.05. Strong winds in August caused the largest increase in open water during the summer melt season with the lead fraction increasing from ~ 0.05 to 0.18 over a period of days. Thus it would appear that lateral melting in leads did not play a significant role in expanding the lead area before the August winds, suggesting that the ice-albedo feedback did not have a large, direct impact on the ice coverage during SHEBA. Even so, accounting for heat absorbed in leads is important for the overall budget of the Arctic ice and underlying ocean mixed layer. As pointed out by *Eicken et al.* [2002], meltwater is in constant flux through the sea ice so that heat and salinity of leads can have a significant impact on surrounding melt ponds and fresh water trapped in pockets beneath the ice. It is likely that melting of the ice pack via meltwater migration between leads and melt ponds contributed to the large increase in lead fraction that accompanied stronger winds in August.

[41] As pointed out by one of our reviewers, observations and modeling results presented here suggest a conceptual lead model where leads act as either isolated, stagnant pools that do not exchange heat with the underlying ocean or as open radiators that provide a conduit for heating the ocean mixed layer. Measurements and simulations indicate that during SHEBA, leads initially acted as radiators but then quickly stratified because of surface meltwater flux. For most of the month of July, leads behaved as stagnant pools where much of the absorbed solar radiation was used to melt the lead edges.

[42] Although lead area fraction did not appear to increase substantially through lateral melting, expansion of fresh water ponds on the ice surface was likely enhanced through edge and bottom melting [*Perovich et al.*, 2002]. For most of the SHEBA summer melt period, fresh water ponds covered 15 to 20 percent of the surface area and were a key element in setting the overall surface albedo. In many ways, fresh water ponds have properties similar to leads capped with a fresh layer or the stagnant pool model described above. Ponds expand through runoff of melting ice and by lateral melting that is most likely dependent on wind forcing and the percolation of meltwater through the surrounding ice [*Eicken et al.*, 2002]. One question that could be important is determining how wind forcing affects melting rates on different sections of the pond. For example, do wind driven circulations help determine if bottom melt is stronger than lateral melt in ponds? Given the results from SHEBA and our simulations, improved representation of ponds in coupled ocean/ice models maybe of greater importance than leads.

[43] **Acknowledgments.** We would like to acknowledge the supercomputer time provided by the National Center for Atmospheric Research, which is funded by the National Science Foundation. This work was supported as part of the Surface Heat Budget of the Arctic (SHEBA) project by National Science Foundation grant OPP-00-84284 and the Office of Naval Research grant N00014-01-1-0022/ORSC.

References

Bitz, C. M., M. M. Holland, A. J. Weaver, and M. Eby (2001), Simulating the ice-thickness distribution in a coupled climate model, *J. Geophys. Res.*, *106*, 2441–2463.

Cheung, T. K., and R. L. Street (1988), The turbulent layer in the water at an air-water interface, *J. Fluid Mech.*, *194*, 133–151.

Eicken, H., H. R. Krouse, D. Kadko, and D. K. Perovich (2002), Tracer studies of pathways and rates of meltwater transport through Arctic summer sea ice, *J. Geophys. Res.*, *107*(C10), 8046, doi:10.1029/2000JC000583.

Holland, M. M., J. A. Curry, and J. L. Schramm (1997), Modeling the thermodynamics of a sea ice thickness distribution: 2. Sea ice/ocean interactions, *J. Geophys. Res.*, *102*, 23,093–23,108.

Maykut, G. A. (1978), Energy exchange over young sea ice in the central Arctic, *J. Geophys. Res.*, *83*, 3646–3658.

McPhee, M. G. (2002), Turbulent stress at the ice/ocean interface and bottom surface hydraulic roughness during the SHEBA drift, *J. Geophys. Res.*, *107*(C10), 8037, doi:10.1029/2000JC000633.

McPhee, M. G., G. A. Maykut, and J. H. Morison (1987), Dynamics and thermodynamics of the ice/upper ocean system in the marginal ice zone of the Greenland Sea, *J. Geophys. Res.*, *92*, 7017–7031.

Perovich, D. K., W. B. Tucker III, and K. A. Ligett (2002), Aerial observations of the evolution of ice surface conditions during summer, *J. Geophys. Res.*, *107*(C10), 8048, doi:10.1029/2000JC000449.

Perovich, D. K., T. C. Grenfell, J. A. Richter-Menge, B. Light, W. B. Tucker III, and H. Eicken (2003), Thin and thinner: Sea ice mass balance measurements during SHEBA, *J. Geophys. Res.*, *108*(C3), 8050, doi:10.1029/2001JC001079.

Skyllingstad, E. D., and D. W. Denbo (2001), Turbulence beneath sea ice and leads: A coupled sea ice/large-eddy simulation study, *J. Geophys. Res.*, *106*, 2477–2498.

Skyllingstad, E. D., C. A. Paulson, W. S. Pegau, M. G. McPhee, and T. Stanton (2003), Effects of keels on ice bottom turbulence exchange, *J. Geophys. Res.*, *108*(C12), 3372, doi:10.1029/2002JC001488.

Tripoli, G. J. (1992), A nonhydrostatic mesoscale model designed to simulate scale interaction, *Mon. Weather Rev.*, *120*, 1342–1359.

C. A. Paulson and E. D. Skyllingstad, College of Oceanic and Atmospheric Sciences, Oregon State University, Corvallis, OR 97331-5503, USA. (cpaulson@oce.orst.edu; skylling@oce.orst.edu)

W. S. Pegau, Kachemak Bay Research Reserve, 3298 Douglas Place, Homer, AK 99603-8027, USA. (spegau@coas.oregonstate.edu)